Refractive Index Enhancement by Secondary Organic Aerosol Formation in Humid Southern China Challenges Model Assumptions

Junlin Shen[1], Ye Kuang[1], Li Liu[2], Fengling Yuan[1], Biao Luo[1], Hongqing Qiao[1], Miaomiao Zhai[1], Gang Zhao[3], Hanbing Xu[4], Fei Li[5], Yu Zou[2], Tao Deng[2], Xuejiao Deng[2], Ye Kuang[1]

[1] Institute for Environmental and Climate Research, College of Environment and Climate, Jinan University, Guangzhou, 511443, Guangdong, China

[2] Guangzhou Institute of Tropical and Marine Meteorology of China Meteorological Administration, GBA Academy of Meteorological Research, Guangzhou, 510640, China.

[3] Key Laboratory of Ecology and Environment in Minority Areas, Minzu University of China, National Ethnic Affairs Commission, Beijing,100081, China

[4] School of Computer Science and Engineering, Sun Yat-Sen University, Guangzhou, 510275, Guangdong, China

[5] Xiamen Key Laboratory of Straits Meteorology, Xiamen Meteorological Bureau, Xiamen, 361012, Fujian, China

Correspondence: Ye Kuang (kuangye@jnu.edu.cn)

Abstract:

Aerosol-radiation interactions play a crucial role in air pollution and climate change with scattering being the dominant process. The complex refractive index of organic aerosols is essential for accurately simulating these interactions, with the scattering capability is predominantly determined by the real part of the refractive index (m_r). Prevailing models often assume a constant m_r for organic aerosols (e.g., 1.53 or 1.45) at different wavelengths or claim that m_r of primary organic aerosols (POA) is substantially higher than that of secondary organic aerosols (SOA) (e.g., 1.63 for POA and 1.43 for SOA), largely due to a lack of direct measurements. This study employs direct measurements from the DMA-SP2 system to demonstrate a strong diameter dependence of dry state m_r at 1064 nm, closely associated with primary aerosol emissions and secondary aerosol formation. Source apportionment of aerosol size distributions reveals that the m_r of SOA is substantially higher than that of POA. Optical closure calculations, based on extensive dry state observations of aerosol scattering at 525 nm, size distributions, and chemical compositions, confirmed that SOA formation would enhance aerosol m_r substantially (from lower than 1.45 when POA dominates to higher than 1.55 when SOA dominates). These results challenge existing model assumptions. In addition, further analysis reveals m_r of SOA increases substantially with oxidation level which is likely associated with multiphase SOA formation. Our analysis recommends m_r values at 525 nm of 1.37 for POA and 1.59 for SOA in urban regions with emissions and meteorological conditions similar to those at the observation site in Guangzhou, a city located in humid southern China. These findings underscore that current modeling practices may introduce substantial inaccuracies in estimating the radiative effects of organic aerosols.

1. Introduction

Aerosol-radiation interactions play a crucial role in air pollution and climate change. Atmospheric aerosols scatter and absorb solar radiation, which can alter the thermal structure of the atmosphere, the radiative energy balance of the Earth-atmosphere system, and affect atmospheric visibility. On one hand, aerosols influence the thermal structure of the surface and atmosphere, which affects the development of the atmospheric boundary layer (Zhong et al., 2019), thereby playing an important role in the evolution of pollution processes and air pollution. On the other hand, by scattering and absorbing solar radiation, aerosols can affect the radiative energy balance of the Earth-atmosphere system, impacting both local and global climates. Due to the complexity of atmospheric aerosol components, the direct radiative effect of aerosols (referred to as aerosol-radiation interactions in the latest IPCC report) is the second-largest source of error in accurately assessing anthropogenic climate forcings (IPCC,AR6, 2023) and is a significant factor limiting the accurate prediction of global climate change.

The inability to accurately characterize the complex refractive index of organic aerosols is one of the major sources of error in accurately simulating the direct radiative effects of aerosols (Redemann et al., 2000;Li et al., 2021;Tsigaridis and Kanakidou, 2018). Organic aerosols are a significant component of atmospheric aerosols, on average accounting for about 20-60% of submicron aerosols in most continental regions (Zhang et al., 2007). In some areas, such as tropical rainforest regions, the organic proportion can be as high as 90% (Kanakidou et al., 2005). Therefore, organic aerosols are one of the main contributors to the direct radiative effects of aerosols and likely a major source of error in accurately assessing these effects (Moise et al., 2015). Compared to inorganic aerosols, the complex chemical composition of organic aerosols poses a core challenge to accurately quantifying their optical properties (Wu et al., 2021). Based on Mie scattering theory, the core parameters affecting aerosol optical properties in dry state are aerosol size and complex refractive index. In both climate models and atmospheric chemical transport models, the complex refractive index is a fundamental parameter for calculating key optical parameters such as the extinction coefficient, single scattering albedo, and asymmetry factor (Moise et al., 2015). The real part (m_r) of the complex refractive index corresponds mainly to scattering properties, while the imaginary part corresponds mainly to absorption properties. The extinction of solar radiation by aerosols is determined by aerosol scattering and absorption with scattering being the dominant process (Moise et al., 2015). Accurately characterizing m_r of organic aerosols ($m_{r,OA}$) is thus key to accurately simulating aerosol radiative effects (Li et al., 2021;McMeeking et al., 2005). The review by Tsigaridis and Kanakidou (2018) pointed out that

82   existing models either treat $m_{r,OA}$ as a constant or treat m_r for POA and SOA ($m_{r,POA}$ and $m_{r,SOA}$) as

83   constants. For example, Curci, et al. (2019) set $m_{r,POA}$ to 1.63 and $m_{r,SOA}$ to 1.43 in their model.

84   However, results from existing literature of laboratory studies demonstrate that $m_{r,OA}$ varies a lot.

85   The advantage of laboratory studies is that they can produce aerosol systems containing only organic

86   components, with a relatively narrow size range, allowing the retrieval of $m_{r,OA}$ based on scattering

87   or extinction measurements. Consequently, laboratory quantitative studies on $m_{r,SOA}$ have been

88   conducted broadly (Moise et al., 2015), while $m_{r,POA}$ are rarely investigated. The results show that

89   the $m_{r,SOA}$ varies mainly in the range of 1.36-1.66, and the variation of $m_{r,SOA}$ is closely related to its

90   precursors and oxidation pathways (Moise et al., 2015;Kim et al., 2014;Lambe et al., 2013;He et al.,

91   2018). For example, results of He et al. (2018) demonstrate that $m_{r,SOA}$ first increase with the oxidation

92   state parameter O/C and then decrease with O/C during the aging. Li et al. (2023c) further developed

93   a parameterization scheme for $m_{r,SOA}$ based on O/C and H/C and validated it using laboratory

94   experiment results, however, its applicability to POA and SOA on the basis of field measurements

95   remains lacking. Overall, the difficulty in direct quantification of $m_{r,OA}$ on the basis of field

96   measurements has made the variation characteristics of $m_{r,OA}$ in the atmosphere remain elusive.

97   In this study, using field measurements of aerosol refractive index, aerosol size distributions,

98   aerosol scattering properties as well as aerosol chemical compositions, the remarkable difference in

99     $m_{r,POA}$ and $m_{r,SOA}$ is revealed. It was found that SOA formation in the observation site would enhance

100   substantially the m_r. These findings serve strong observational evidence that $m_{r,SOA}$ is much higher

101   than $m_{r,POA}$ in many regions and values for model settings of $m_{r,POA}$ and $m_{r,SOA}$ are recommended

102   on the basis of observations.

103   **2. Materials and Methods**

104   **2.1 Field measurements**

105   In this study, we utilized datasets from two field campaigns conducted at Haizhu Wetland Park,

106   Guangzhou, China. The first campaign lasted less than two months, from January 12 to February 27,

107   2022, while the second was a longer-term campaign spanning approximately seven months, from July

108   27, 2022, to February 28, 2023.

109   During the first campaign, we observed the particle number size distribution (PNSD) in a dry

110   state, ranging from 13 nm to 800 nm, using a Scanning Mobility Particle Sizer (SMPS, model 3086

111   and particle counter 3776 from TSI) with a temporal resolution of 5 minutes. The m_r of BC-free

112   aerosols with diameters of 235 nm, 270 nm, 300 nm, 335 nm, 370 nm, and 400 nm were measured

113   using the DMA-SP2 system (differential mobility analyzer in tandem with single-particle soot

114   photometer from Droplet Measurement Technologies, Boulder, Colorado (Schwarz et al., 2006)). This

115   measurement method for m_r was previously proposed by Zhao et al. (2019c). To briefly explain the

116   m_r measurement using the DMA-SP2 system: the SP2 channels receive both scattering and

117   incandescent signals from sampled aerosols. For pure scattering aerosols, the peak of the scattering

118   signal is positively correlated with aerosol scattering ability, which is determined by aerosol size and

119   m_r for spherical particles. The scattering strength (S) at 1064 nm can be expressed as (Zhao et al.,

120   2019c):

121    $S = C \times I_0 \times \sigma \times (PF_{45°} + PF_{135°}),$

122   Where I_0 is the instrument's laser intensity, C is a constant determined by the instrument's response

123   characteristics, σ is the scattering coefficient of aerosols, $PF_{45°}$ and $PF_{135°}$ are the scattering phase

124   functions at 45° and 135°, respectively. The relationship between the peak of the scattering signal and

125   the scattering strength of pure scattering aerosols has been calibrated using ammonium sulfate (see

126   Sect. S1 of the supplement). Consequently, the m_r at 1064 nm (m_{r1064}) of SP2 laser for pure scattering

127   aerosols can be retrieved using the particle size from the DMA and the scattering strength from the

128   SP2, following the method demonstrated by Zhao et al. (2019c). The DMA-SP2 technique offers the

129   advantage of providing direct measurements of m_{r1064}. However, it also has certain limitations. For

130   instance, in this study, the m_{r1064} measurements are constrained to a diameter range of approximately

131   235 to 400 nm, depending on laser intensity, thereby excluding smaller particles (<200 nm) and

132   relatively larger submicron particles (>400 nm). Additionally, some BC-free particles exhibit

133   absorptive properties, such as brown carbon containing particles that may absorb at infrared

134   wavelengths (Hoffer et al., 2017). Thus, these particles may absorb laser energy during scattering

135   measurements, causing heating that can lead to the evaporation of semi-volatile or even low-volatile

136   species from the particle phase, potentially biasing the m_{r1064} measurements. Although this effect is

137   likely very small because this type of brown carbon aerosols likely account for very small portions of

138   BC-free aerosols (Luo et al., 2022). Non-refractory submicron (NR-PM$_1$) aerosol chemical

139   compositions—including ammonium (NH4), nitrate (NO3), sulfate (SO4), chloride (Cl), and organic

140   components—were measured using a Quadrupole Aerosol Chemical Speciation Monitor (Q-ACSM).

141   Aerosol absorptions at multiple wavelengths were measured using the AE33 from MAGEE (Drinovec

142   et al., 2015). Note that a PM$_{2.5}$ inlet (BGI, SCC 2.354) with a required flow rate of 8 L/min was used

143   for aerosol sampling, with a Nafion drier of 1.8 m length downstream of the impactor, which ensures

144   the sampling RH in instruments could be down to around 10% as recorded by the inlet RH sensor of

145   the Q-ACSM. The flow rates of the Q-ACSM, SMPS, SP2 and AE33 instruments were set to 3 L/min,

146   0.3 L/min, 0.1 L/min, and 5 L/min, respectively. Nafion drier and all sampling tudes before instruments

147   were placed vertically to reduce sampling loss. Details about the quality assurance of Q-ACSM

148   measurements during this campaign are provided by Li et al. (2023a).

149   During the second campaign, direct measurements of m_{r1064} were not conducted. Instead, dry

150   state aerosol scattering coefficients of total suspended particles (TSP) at 450, 525, and 635 nm were

151   measured using a nephelometer (Aurora 3000 from Ecotech, (Müller et al., 2011)) under nearly dry

152   conditions (below 15% relative humidity). The dry-state (relative humidity below 20%) PNSD,

153   ranging from 13 to 800 nm, was again measured using the SMPS. Additionally, multi-wavelength

154   aerosol absorption measurements were performed using an AE33 Aethalometer (Drinovec et al.,

155   2015), and the NR-PM$_1$ aerosol chemical compositions were also measured using the Q-ACSM.

2.2 Source Analysis Methods of Organic Aerosols and Aerosol Size Distributions

157   The multilinear engine (ME-2) technique (Canonaco et al., 2013;Canonaco et al., 2021) was

158   applied to the organic aerosol mass spectra to resolve the sources of organic aerosols. Multilinear

159   Engine (ME-2) is an upgrade of widely used Positive Matrix Factorization (PMF) technique and runs

160   on an IGOR-based interface (Canonaco et al., 2013). Different from traditional PMF, ME-2 offers

161   capability of constraining the spectra variation extent of OA factor with given priori mass spectra

162   (Canonaco et al., 2013;Guo et al., 2020). Four factors were identified across both field campaigns: two

163   primary organic aerosol (POA) factors and two secondary organic aerosol (SOA) factors. The POA

164   factors consisted of hydrocarbon-like organic aerosol (HOA) and cooking-like organic aerosol (COA),

165   while the SOA factors consisted of less oxygenated organic aerosol (LOOA) and more oxygenated

166   organic aerosol (MOOA). The spectral profiles of HOA and COA obtained in Liu et al. (2022) were

167   used in the ME-2 procedure to constrain POA factor variations.

168   The POA factors exhibited consistent spectral profiles and elemental ratios between the two

169   campaigns. For example, the O/C ratios of HOA were 0.16 and 0.17, and the O/C ratios of COA were

170   0.12 and 0.14, respectively. However, the resolved SOA factors differed between the campaigns. The

171   O/C ratio of LOOA in the short-term campaign was 0.89, while it was 0.60 in the long-term campaign.

172   Similarly, the O/C ratio of MOOA was 0.93 in the short-term campaign and 1.27 in the long-term

173   campaign. These differences do not affect the overall analysis of this study, as the focus is primarily

174   on the distinction between POA and SOA. More details about the source analysis of organic aerosols

175   can be found in the supplements of Li et al. (2023a) for the short-term campaign and Qiao et al. (2024)

176   for the long-term campaign.

177   Additionally, following PMF procedure for the PNSD measurements and the source
178   apportionment method introduced by Cai et al. (2020a), five PNSD factors were identified (PMF 2,
179   ver. 4.2, 111 bins for PNSD ranging from 14 nm to 736 nm as inputs). For details on the determination
180   of the factor numbers and the PNSD factor analysis, please refer to Sect. S2 of the supplement. In the
181   source apportionment of PNSD factors, ammonium, nitrate, and sulfate measurements were paired as
182   ammonium sulfate (AS) and ammonium nitrate (AN) using the scheme proposed by Gysel et al. (20)
183   considering that different impacts of AS and AN formation on PNSD. The mass concentrations of
184   refractory black carbon (rBC) during the short-term campaign were integrated from size-resolved rBC
185   measurements obtained using the DMA-SP2 system, as described in Li et al. (2023a). Correlation
186   analysis between mass concentrations of OA factors, rBC, AS as well as AN and resolved PNSD
187   factors were performed to help explore sources of different PNSD factors.

188   In addition, the densities of aerosol species used for volume calculations in this study were
189   consistent with those in Kuang et al. (2021): 1.78 g/cm³ for AS and AN, 1.0 g/cm³ for HOA and COA,
190   1.2 g/cm³ for LOOA, and 1.4 g/cm³ for MOOA. However, 1.0 g/cm³ was chosen for rBC on the basis
191   of previous observations results (Zhang et al., 2016b;Zhao et al., 2020;Zhou et al., 2022). Calculating
192   BC volume for hygroscopicity requires the material density of BC, as described in Kuang et al. (2021).
193   However, for Mie calculations in this study, effective BC density is needed to determine the BC core
194   size. Since the presence of air voids (Zhang et al., 2016b;Zhao et al., 2020) within BC particles
195   increases their apparent size compared to calculations based on the material density. The source
196   analysis of resolved PNSD factors through combination of ACSM measurements was discussed
197   comprehensively in Sect 3.1 to help explore observed m_r diameter dependence.

198   **2.3 Optical Closure and associated m_r Retrieval**

199   During the second long-term field campaign, dry-state aerosol scattering coefficients of TSP and
200   PNSD (ranging from 13 to 800 nm, generally covering dry-state PM1), as well as BC mass
201   concentrations, were simultaneously measured, making it feasible to perform a closure between the
202   measured and simulated aerosol scattering ($\sigma_{sp,obs}$ vs $\sigma_{sp,sim}$). Details about aerosol scattering
203   calculating procedures and simulations using the Mie code of BHCOAT (Bohren and Huffman,
204   1998;Cheng et al., 2009) could be found in Sect. S4. Five key issues needed to be addressed for this
205   closure: (1) The size range mismatch between aerosol scattering measurements (TSP) and PNSD
206   measurements (dry-state PM1); (2) BC mass size distributions and mixing state, and other BC related
207   parameters such as density and refractive index; (3) The m_r of BC-free aerosols at 525 nm; (4)
208   Imaginary part of BC-free aerosols which is mostly associated with brown carbon; (5) Corrections for

209   integrating nephelometer measurements to account for truncation errors and light source non-idealities

210   (Müller et al., 2011).

211   Recent field observations (detailed in Sect. S3 of the supplement), utilizing a system (Kuang et

212   al., 2024) that coupled different aerosol inlets with a integrating nephelometer, demonstrated that in

213   Guangzhou's urban area, scattering coefficients of dry-state PM_1 and TSP (σ_{sp,PM_1} vs $\sigma_{sp,TSP}$)

214   generally agree well (Fig. S4a, R = 0.99). However, their ratio varies substantially depending on

215   aerosol scattering levels (Fig. S4b). Specifically, the ratio $\sigma_{sp,TSP}/\sigma_{sp,PM_1}$ at 525 nm exceeds 1.2 when

216    $\sigma_{sp,TSP}$ is below 50 Mm^{-1}, reaching approximately 1.5 when $\sigma_{sp,TSP}$ is around 10 Mm^{-1}. This ratio

217   decreases as $\sigma_{sp,TSP}$ increases and stabilizes (near 1.08) when $\sigma_{sp,TSP}$ exceeds 90 Mm^{-1}. Consequently,

218   for the closure, measured dry-state $\sigma_{sp,TSP}$ was corrected to dry-state σ_{sp,PM_1} using the observed

219    $\sigma_{sp,TSP}$-dependent relationship shown in Fig. S4b (ratio of 1.08). This ratio may vary across seasons.

220   However, aerosol scattering simulation results based on particle size distribution measurements that

221   cover the supermicron range, conducted during six campaigns across various locations and seasons in

222   the North China Plain, indicate that PM_1 on average contributes approximately 90% to TSP scattering

223   (Fig. 2 of Kuang et al. (2018)). This aligns closely with the average ratio of 1.08 determined in this

224   study through direct scattering measurements, suggesting that this ratio likely does not vary

225   substantially.

226   The BC mass size distributions and mixing state during the first short-term campaign were

227   analyzed systematically in a previous study conducted by Li et al. (2023a). Two key findings emerged:

228   (1) BC mass size distributions for diameters >100 nm could be represented by a single lognormal mode,

229   with a geometric mean diameter (D_g) of 258 (±16) nm and a geometric standard deviation (σ_g) of 1.69;

230   (2) Nearly half of the BC mass was identified as externally mixed. The mass fraction of externally

231   mixed BC in total BC (R_{ext}) was calculated as 0.56 ± 0.16, and the number fraction (R_{csm}) of internally

232   mixed BC (represented by the core-shell model) in total number of internally mixed BC and BC-free

233   particles was 0.13 ± 0.12. These findings indicated that, despite clear evidence of secondary aerosol

234   formation during the first campaign, BC mass size distributions and mixing states varied within a

235   relatively narrow range, primarily influenced by traffic emissions (Li et al., 2023a). Therefore, the

236   parameters D_g= 258 nm, σ_g= 1.69, R_{ext}= 0.56, and R_{csm}= 0.13 were used to distribute the BC mass

237   concentrations measured by the AE33 and account for BC mixing states. In brief, aerosol particles were

238   divided into three types: externally BC, internally mixed BC with BC as the core, and BC-free. BC

239   mass was distributed into different diameters using the established lognormal function, and further

240   allocated to externally and internally mixed BC-containing particles using parameters R_{ext} and R_{csm}.

241 Note that these values regarding BC size distributions and mixing states are not expected to remain

242 constant throughout the campaign. However, sensitivity test conducted on the basis of observations in

243 the short campaign help boost the confidence. Sensitivity test results shown in Fig.S5 show that even

244 if the geometric mean diameter of the BC mass size distribution changes from 180 nm to 600 nm, very

245 large variation according to reported distribution in literatures (Zhao et al., 2019b), the relative changes

246 in scattering calculations remain relatively small (~2%). Instead, the BC mixing state plays a more

247 critical role. For example, changing the mixing state from completely externally mixed to a fully core-

248 shell internal mixture results in changes of approximately 10%. However, such a scenario represents

249 an extreme condition. Considering the observation site is located near BC source regions, BC aerosols

250 are likely closer to being externally mixed. Errors associated with the BC mixing state parameter are

251 estimated to be less than 2.5%. This inference assumes that BC mixing states in this region vary from

252 completely externally mixed to half externally mixed (much larger than observed in the first short

253 campaign). Using an average value in this case would result in uncertainties of less than 2.5%. Errors

254 associated with BC mixing state would likely be smaller. In addition, other BC related parameters

255 might also induce retrieval errors, such as uncertainties associated with BC density, BC mass and BC

256 refractive index. Especially, the BC mass concentrations derived from AE33 measurements would

257 bear uncertainties associated with variations in mass absorption coefficient (Zhao et al., 2021b).

258 Sensitivity tests about these parameters are also included in Fig.S5. Results of previous study reveal

259 the refractive index of BC has almost minimal impact on scattering calculations (Ma et al., 2012a).

260 This is confirmed by the sensitivity test results shown in Fig. S5, with variations in possible reported

261 ranges of BC refractive index induce variations less than 2%. Results also show that uncertainties in

262 BC mass concentrations and BC density would only induce small scattering changes (near or less than

263 1%).

264 Note that, the sensitivity results shown here is somehow contrary to the conclusion draw by

265 Zhao et al. (2019b) that BC mass size distributions should have comparable impacts with BC mixing

266 states on simulations of aerosol scattering. This was further explored in Sect. S5. The results

267 demonstrate that the simulations in Zhao et al. (2019b) assumes all aerosols contain BC, which is

268 not the case in ambient atmosphere, details about this discussion could be found in Sect. S5.

269 In this region, both primary and secondary aerosols contribute to aerosol absorption (Yuan et al.,

270 2016;Luo et al., 2022), which affect imaginary refractive index part (m_i) of BC-free aerosols. The

271 sensitivity tests about impacts of m_i on scattering calculations were also included in Fig.S5. It shows

272 that varying m_i from 10^{-2} to 10^{-7} (reported m_i for different types of brown carbons (Saleh, 2020)) could

273 result in scattering changes of ~5%. However, even for biomass burning organic aerosols which are

274   the most absorbing aerosol type, their m_i at 525 nm is on the order of 10^{-2}. The BC-free aerosol type

275   this campaign mostly consist of inorganic and secondary organic aerosols. The overall m_i of BC-free

276   aerosols are less than 10^{-3} estimated using the brown carbon absorption at 520 nm observed during the

277   campaign even when biomass burning activities prevail (Luo et al., 2022), meaning that scattering

278   deviations induced by errors m_i in assumption are less than 1% for assuming m_i of 10^{-7}.

279   Truncation errors and light source non-idealities were accounted for in the Mie calculations by

280   applying angular light intensity correction functions from Müller et al. (2011). Details of the Mie

281   theory calculations for the optical closure can be found in Sect. S4 of the supplement. Sensitivity tests

282   (discussed in Sect. 5 of the supplement) and above-mentioned discussions make it clear that m_r is the

283   most influential parameter affecting the variations in aerosol scattering calculations.

284   Therefore, the optical closure calculations could be conducted iteratively to retrieve an m_r value

285   that align simulated aerosol scattering at 525 nm with the measured scattering at the same wavelength

286   (Sect. S4). This retrieved m_r at 525 nm, obtained through optical closure, is termed m_{rc525}. The

287   sensitivity tests results shown in Fig.S7 demonstrate the accuracy of σ_{sp,PM_1} conversion from

288   represents one of the most important factors that would influence the accuracy of retrieved m_{rc525}.

289   The accuracy of σ_{sp,PM_1} depends largely on the accuracy of ratio used for converting measured $\sigma_{sp,TSP}$

290   to σ_{sp,PM_1} as discussed. Large standard deviation of the ratio $\sigma_{sp,TSP}/\sigma_{sp,PM_1}$ (>10%) exist for data

291   points of $\sigma_{sp,TSP}$ at 525 nm below 50 Mm^{-1} (shown in Fig. S4b). For these points, even if correcting

292   the inlet inconsistency with the average curve shown in Fig.S4, large uncertainty would inevitably be

293   introduced to the optical closure. Therefore, m_{rc525} was only retrieved when $\sigma_{sp,TSP}$ at 525 nm

294   exceeded 50 Mm^{-1} (~75% of data points), where the ratio between σ_{sp,PM_1} and $\sigma_{sp,TSP}$ varied with

295   standard deviations less than 5% (Fig.S4).

296   **3 Results and discussions**

297   **3.1 Strong Diameter Dependence of m_{r1064} and Remarkable Difference in $m_{r,POA}$ and $m_{r,SOA}$**

298   **Revealed by Direct m_{r1064} Measurements**

299   During the first campaign, significant variations in the m_{r1064} were revealed using DMA-SP2

300   measurements (Fig. S9), with m_{r1064} values ranging from 1.40 to 1.59 (mean: 1.49 ± 0.03). Fig.1a and

301   1b illustrate the diameter-dependent characteristics of the measured m_{r1064}. Aerosols larger than 300

302   nm generally exhibited higher m_{r1064} values compared to those smaller than 300 nm, with average

303   m_{r1064} values at diameters of 253 nm, 270 nm, 300 nm, 335 nm, 370 nm, and 400 nm being 1.46,

304   1.49, 1.48, 1.51, 1.51, and 1.51, respectively. This is consistent with previous findings indicating a

305   clear diameter dependence, where m_{r1064} tends to increase with particle diameter (Benko et al.,

306   2009;Zhao et al., 2019a). Using the m_{r1064} ratio between 400 nm and 235 nm ($m_{r1064,400}/m_{r1064,235}$)

307   as an indicator of m_{r1064} diameter dependence, we found that this ratio increases with $m_{r1064,400}$ (Fig.

308   1b). Specifically, the ratio $m_{r1064,400}/m_{r1064,235}$ rose from 1.02 to 1.07 as $m_{r1064,400}$ increased from

309   1.46 to 1.58, while $m_{r1064,235}$ showed only a slight increase from 1.45 to 1.47. This suggests that the

310   chemical processes responsible for the increase in $m_{r1064,400}$ have minimal influence on the chemical

311   properties of aerosol particles near 235 nm. Indicating that variations in $m_{r1064,400}$ and $m_{r1064,235}$ are

312   governed by different chemical and emission processes. The aerosol chemical compositions of NR-

313   PM$_1$ presented in Fig. 1b reveal that the condition corresponding to $m_{r1064,400}$ of 1.56 has an overall

314   higher content of MOOA than that near $m_{r1064,400}$ of 1.48. This is further confirmed by the probability
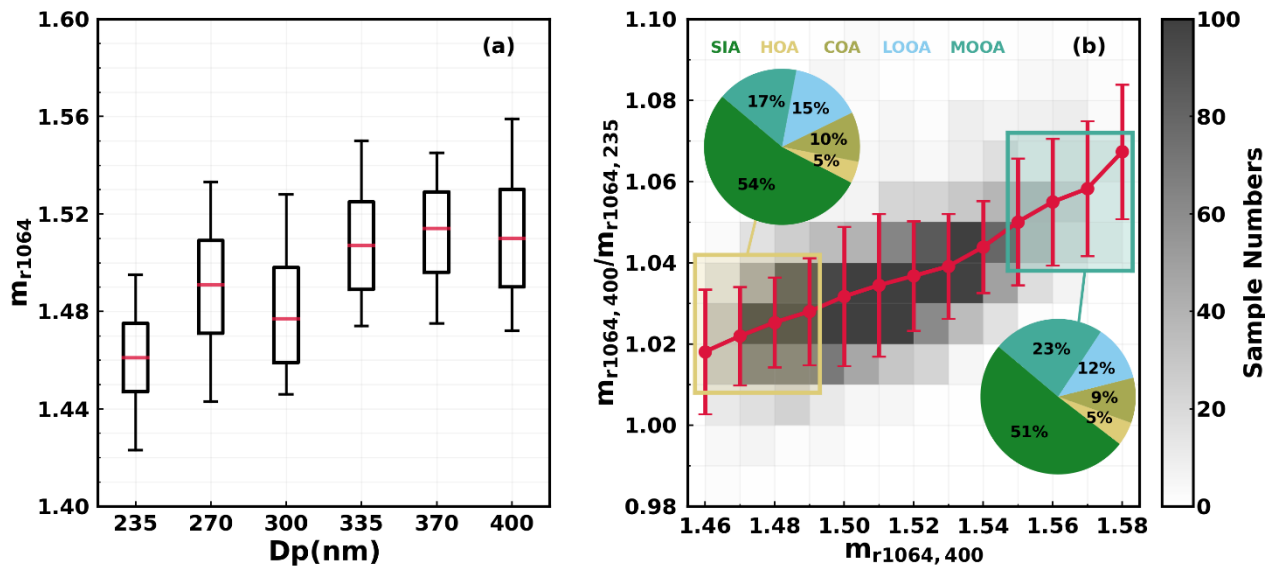
Figure 1. **(a)** The box-and-whisker plot (5th, 25th, 75th and 95th percentiles) of m_{r1064} at different diameters; **(b)** Variations of $m_{r1064,400}/m_{r1064,235}$ under different $m_{r1064,400}$ levels, the intensity of colors indicating the numbers of samples, while red spots and error bars represent average values and standard deviations. Pie charts corresponding average aerosol compositions under different $m_{r1064,400}$ ranges.

315   distribution of MOOA mass fractions in two regions of Fig.1b shown in Fig.S10. Although size

316   distribution of secondary aerosols matter, this general result suggests that secondary organic aerosol

317   formation has possibly contributed to the substantial increase in $m_{r1064,400}$. However, these results

318   reflect bulk compositional changes that may differ considerably from changes in composition fractions

319   at 400 nm. ~~Overall~~ Also, these findings ~~indicate~~suggest that ~~aerosols with diameters~~the chemical

320   processes responsible for the increase in $m_{r1064,400}$ have minimal influence on the chemical properties

321   of aerosol particles near 235 nm, and ~~400 nm likely originate from distinct sources, and~~that variations

322 in $m_{r1064,235}$ and $m_{r1064,400}$ ~~might reveal m_r characteristics of~~ are governed by different ~~aerosols~~
323 ~~sources.~~ chemical and emission processes.

324   As introduced in the previous section, the PMF source apportionment technique was applied to
325 aerosol chemical composition measurements and aerosol volume size distribution measurements
326 during the first short-term field campaign. Results of these two approaches were combined to resolve
327 the chemical fingerprints of sources at different diameters. The average mass fractions during this
328 campaign are as follows: POA (HOA + COA) at 15.4%, SOA (LOOA + MOOA) at 34.7%, ammonium
329 nitrate (AN) at 26.8%, and ammonium sulfate (AS) at 23.2%, demonstrating a dominant contribution
330 from secondary sources. Fig.2a illustrates the average volume size distributions of five resolved factors
331 based on PNSD measurements. It shows that aerosols at a diameter of 235 nm are primarily contributed
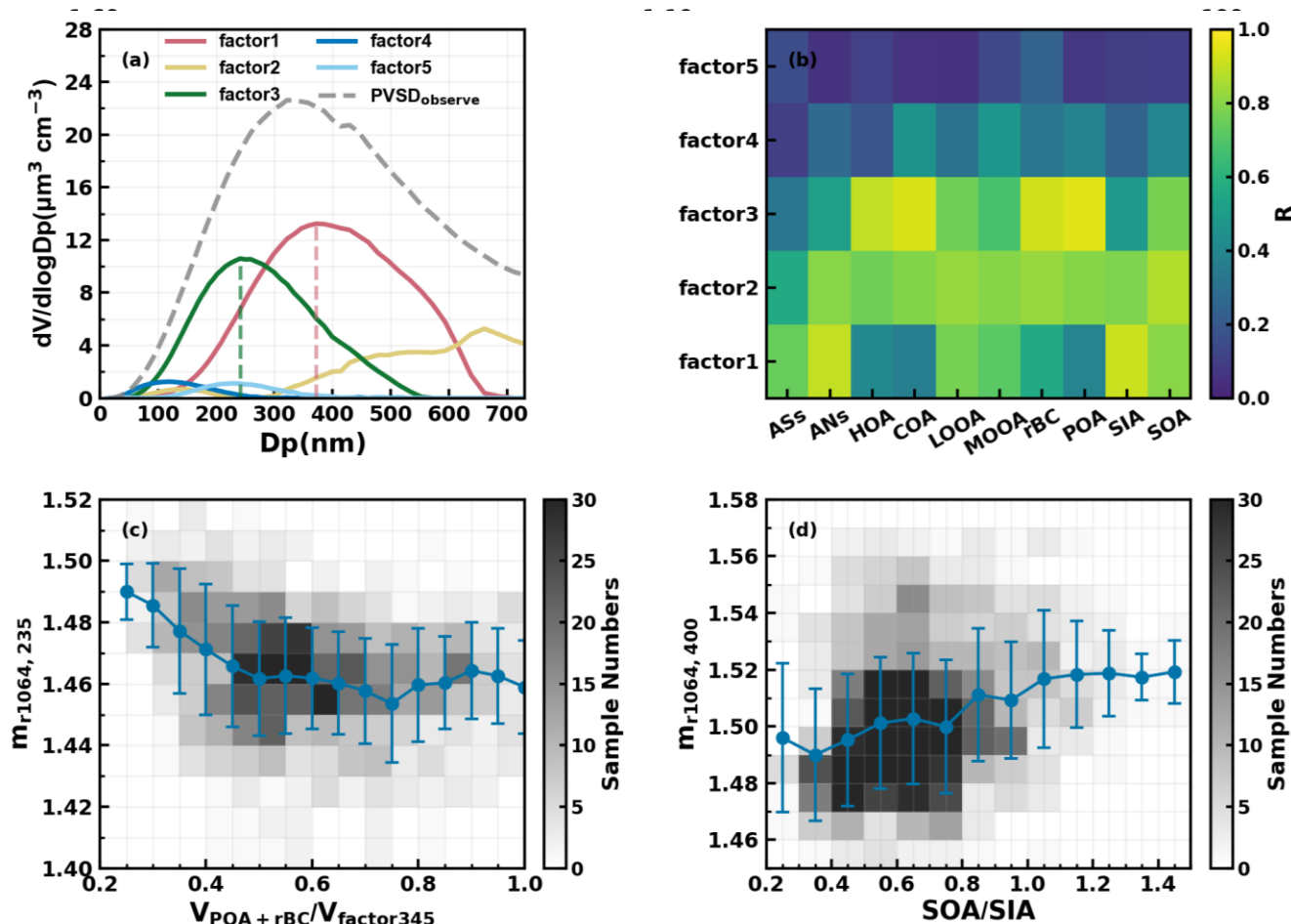
Figure 2. **(a)** The volume size distributions of factors from PNSD PMF analysis; **(b)** Correlation coefficient between volume concentrations of chemical compositions and resolved PNSD size factors; **(c)** $m_{r1064,235}$ varies with changes in the ratio of volume sum of POA and rBC to the volume sum of factor3, factor4 and factor5 (factor 345); **(d)** $m_{r1064,400}$ varies with SOA to SIA when mass summation of factor1 and factor 2 account for over 70% at 400 nm. The intensity of colors indicates the numbers of samples, while red spots and error bars represent average values and standard deviations in **(c)** and **(d)**.

by factors 1, 3, and 5, with factor 3 being the most significant contributor. In contrast, aerosols at 400 nm are mainly contributed by factors 1, 2, and 3, with factor 1 as the dominant contributor.

Cai et al. (2020a) introduced an analytical method linking resolved aerosol size distributions to different sources obtained from mass spectrometer measurements; this method is adopted here. The correlation coefficients for mass concentrations of different aerosol sources and volume of different factors are shown in Fig.2b. For factor 1, the volume peak size is around 400 nm, contributing an average of 58% to the total measured aerosol volume, and shows a strong correlation with secondary inorganic aerosols (SIA, R = 0.91), as well as a notable correlation with SOA (R = 0.80). Factor 2 contributes an average of 5.61% to the total volume and exhibits the highest correlation with SOA (R = 0.87). The correlation analysis indicates that factors 1 and 2 are indeed linked to secondary sources, with the correlation coefficient between the volume sums of factors 1 and 2 and the mass concentrations of secondary components (SIA + SOA) reaching as high as 0.95. Taken together, these findings suggest that secondary organic and inorganic particulate matter are dominant components in particles larger than 400 nm, consistent with previous observations that larger particles are generally more aged than smaller ones (Sun et al., 2012;Xu et al., 2021).

The volume size distribution of factor 3 ranges from 40 nm to 500 nm, with a geometric mean diameter of approximately 240 nm, contributing 46% to the total volume concentration. It shows strong correlations with HOA (R= 0.89), COA (R = 0.93), and rBC (R = 0.92). This finding aligns with previous studies, which indicate that the peak volume size for HOA, COA, and rBC from traffic emissions, typically occurs between 200 nm and 300 nm (Cai et al., 2020b;Sun et al., 2012;Xu et al., 2021;Li et al., 2023a). Furthermore, the correlation coefficient between the volume of factor 3 and the total mass concentrations of HOA, COA, and rBC reaches 0.95, suggesting that factor 3 is predominantly associated with primary aerosol emissions. In addition, both factors 4 and 5 exhibit smaller volume size distributions, collectively contributing 12% to the total volume in the 20 nm to 500 nm range. Although the volume contributions of factors 4 and 5 are generally minor, as shown in Fig. 2a, their diurnal volume variations (illustrated in Fig. S3) and correlations with primary HOA, COA, and rBC are consistently higher than their correlations with secondary species (Fig. 2b). This suggests that factors 4 and 5 are more likely linked to primary sources.

Moreover, the total volume concentrations of factors 3, 4, and 5 are generally consistent with the total volume derived from the mass concentrations of HOA, COA, and rBC (5.8 vs. 6.1 $\mu m^3/cm^3$). However, in 53% of cases, the volume concentrations of factor 3 exceed those derived from the measurements of HOA, COA, and rBC, indicating that factor 3 may sometimes include contributions

364 from other secondary sources, despite primary sources being dominant in most instances. Additionally,

365 as shown in Fig. 2a, while factors 3, 4, and 5 primarily contribute to the mass of aerosols with a

366 diameter of 235 nm, factor 1 also plays a significant role. This suggests that both primary emissions

367 and secondary aerosol formation influence variations in $m_{r1064,235}$. In contrast, variations in

368 $m_{r1064,400}$ are predominantly controlled by secondary aerosol sources, with primary emissions playing

369 a much lesser role. The differing sources of aerosols at diameters of 235 nm and 400 nm, along with

370 the distinct variation characteristics of $m_{r1064,235}$ and $m_{r1064,400}$, may provide insights into m_r

371 differences of POA and SOA.

372 Based on the PNSD PMF results, the volume contribution of factor 3 at a diameter of 235 nm

373 ranges from below 1% to nearly 99%, with an average of 60%. In comparison, the volume contribution

374 of factor 1 varies between nearly 0% and 93%, averaging around 30%. Fig.2c illustrates the variations

375 of $m_{r1064,235}$ as a function of the ratio between the total volume of POA and rBC and the total volume

376 of factors 3, 4, and 5 (referred to as factor 345) under conditions where volume of factor345 dominates

377 at 235 nm (volume fraction greater than 75%). The results indicate that as the contributions of POA

378 and rBC increase within factor 345, $m_{r1064,235}$ decreases from approximately 1.49 to about 1.46 when

379 their volume fraction exceeds 0.5, subsequently fluctuating within a narrow range (1.46 ± 0.02). This

380 suggests that $m_{r1064,POA}$ is likely substantially lower than 1.46, considering that other secondary

381 species contribute more than 30% to aerosol volume at 235 nm under these conditions.

382 Both primary and secondary sources contribute to aerosols of 400 nm, however, volume fractions

383 of factor 1 plus 2 at 400 nm varied between near zero and 99% with an average of 61%, demonstrating

384 that aerosols at 400 nm composed primarily of SIA and SOA, thus variations in SOA and SIA mainly

385 control changes in $m_{r1064,400}$. With regard to m_r values of AS and AN, m_r of AS is consistently

386 reported as 1.53 (Tang, 1996;Stelson, 1990;Lide, 2004), while reported m_r values of AN varied in a

387 relatively large range of 1.41 to 1.56 (Jarzembski et al., 2003;Lide, 2004;Ouimette and Flagan,

388 1982;Schuster et al., 2005;Zhang et al., 2012). However, known m_r values of AS and AN demonstrate

389 that it is likely not the formation of SIA that has led to $m_{r,400}$ to be as high as 1.58, and could most

390 possibly result from SOA formations, and results of previous laboratory (Li et al., 2017) and field

391 studies (Zhao et al., 2021a) suggested that SOA formations might enhance m_r to reach beyond 1.6.

392 However, the direct subtraction of $m_{r1064,SOA}$ with current measurements is quite challenging due to

393 that the lack of size distribution measurements of aerosol chemical compositions. To give a glimpse

394 into the influences of SOA, the variations of $m_{r1064,400}$ under different mass ratios of SOA to SIA are

395 shown in Fig.2d. It shows that on average, $m_{r1064,400}$ indeed increases as a function of SOA fraction,

396 confirming that the $m_{r1064,SOA}$ is higher than those of SIA. Especially, the $m_{r1064,400}$ showed

397 obviously higher correlations with MOOA (R=0.25, p<0.01) than with LOOA (R=-0.24, p<0.01)

398 (Fig.S11), demonstrating that the higher m_r of MOOA than LOOA, and the m_r of LOOA is likely

399 close to those of SIA on the basis of results shown in Figure.S8b. Results of a few existing field

400 measurements supports the finding. For example, results of Aldhaif et al. (2018) suggested that $m_{r,OA}$

401 were likely positively correlated with the O/C. Results of Liu et al. (2022) revealed much stronger

402 scattering abilities of MOOA which likely cannot be solely explained by larger size of MOOA. Li et

403 al. (2023b) established a semi-empirical model to predict the $m_{r,OA}$ from O/C and H/C which was

404 partly confirmed using their laboratory measurements. On the basis of this model and element ratios

405 of OA factors, m_r values for retrieved HOA, COA, LOOA, and MOOA during the first campaign are

406 1.48, 1.48, 1.45, 1.63, respectively, which is partly consistent with the field finding of this research

407 that $m_{r,POA}$ has remarkable difference with $m_{r,SOA}$ with m_r of MOOA is substantially higher,

408 however, the m_r values for HOA, COA might be overestimated by the scheme of Li, et al. (2023b).

409 **3.2 Optical Closure Confirm Remarkably higher $m_{r,SOA}$ than $m_{r,POA}$**
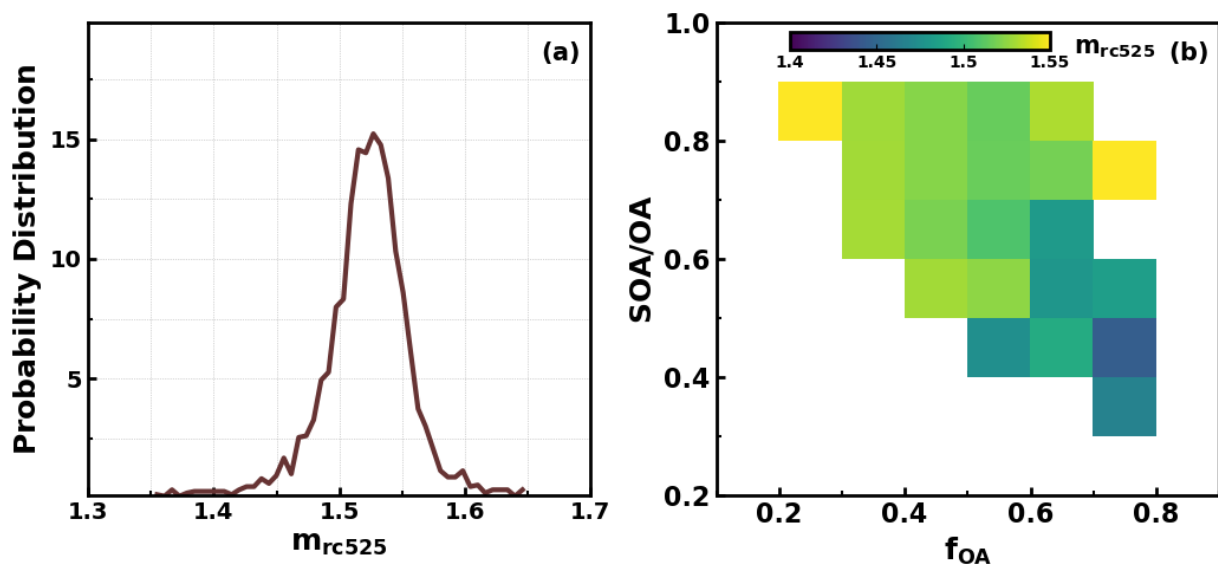
Figure 4. **(a)** Probability distribution of m_{rc525}; **(b)** Variations of m_{rc525} under different OA mass fractions in NR-PM$_1$ (f$_{OA}$) and SOA mass fractions in total OA (SOA/OA).

410 The probability distributions of retrieved m_{rc} using the optical closure method presented in Sect

411 2.3 is presented in Fig.3a, m_{rc525} generally ranges between 1.4 and 1.6 with an average of 1.52. This

412 average m_{rc525} is close to the value of 1.53 typically used in optical closure studies on the basis of

413 field measurements (Ma et al., 2011;Wexler and Clegg, 2002), and also generally consistent with the

414 previously reported m_r range in Guangzhou (Zhang et al., 2016a). The retrieved m_{rc525} is a parameter

415 that represents the bulk m_r of ambient aerosols, therefore, containing influences of both organic and

inorgaic components. To further reveal possible effects of POA and SOA on m_{rc525} variations, average m_{rc525} under different OA mass fractions in NR-PM$_1$ and SOA fractions in OA are presented in Fig.3b. A general characteristic revealed that when OA accounts for more than 50% of NR-PM$_1$, m_{rc525} tends to be lower as mass fraction of POA increase, suggesting that increases in POA would generally lower the m_{rc525}. The fact that m_{rc525} would be even lower than 1.45 when POA dominates, suggesting that $m_{rc525,POA}$ is likely lower than 1.45 which is consistent with the finding revealed in Sect 3.1 that $m_{r1064,POA}$ should be lower than 1.46. Results of Liu et al. (2013) revealed that small m_r wavelength dependence of organic aerosols for wavelengths higher than 500 nm. The finding about $m_{rc525,POA}$ and $m_{r1064,POA}$ here demonstrates that both optical closure calculations and DMA-SP2 measurements reveal same results on the value of $m_{r,POA}$. However, as SOA dominates in OA, the m_{rc525} is enhanced to more than the average of 1.52, suggesting that the $m_{rc525,SOA}$ is at least higher than 1.52 considering that m_{r525} of AS and AN is close to or lower than 1.52. These results qualitatively confirmed the finding in Sect 3.1 that $m_{r,SOA}$ is substantially higher than $m_{r,POA}$.

The complex compositions of ambient aerosols and complex mixing states and refractive index mixing rule (Liu and Daum, 2008;Zhao et al., 2019a) result in the fact that retrieving $m_{r,SOA}$ and $m_{r,POA}$ on the basis of direct m_{rc525} measurements and aerosol composition measurements is extremely challenging (Zhao et al., 2022). Actually, $m_{r,SOA}$ and $m_{r,POA}$ are never reported on the basis of field measurements. Volume mixing rule was first applied in this study to all retrieved m_{rc525} points and corresponding aerosol chemical compositions to tentatively retrieve $m_{rc525,SOA}$ and $m_{rc525,POA}$. The multilinear regression formula with the volume mixing rule could be expressed as $m_{r525} = \varepsilon_{AN} \times m_{rc525,AN} + \varepsilon_{AS} \times m_{rc525,AS} + \varepsilon_{POA} \times m_{rc525,POA} + \varepsilon_{SOA} \times m_{rc525,SOA} + \varepsilon_{AC} \times m_{rc525,AC}$, where ε represents volume fraction of each species in total measured NR-PM$_1$, ε_{AC} represents volume fraction of ammonium chloride by assuming all measured chloride mass is ammonium chloride. In this formula, the $m_{rc525,AS}$ and $m_{rc525,AC}$ is set to 1.53 and $m_{rc525,AN}$ is set to 1.5 (a middle value reported in the literatures) in the retrieval in terms of existing literatures as listed in Sect 3.1. As shown in Fig.4a, if all retrieved m_{rc525} points were used, $m_{rc525,POA}$ and $m_{rc525,SOA}$ of 1.45 and 1.54 could be retrieved (using python curve_fit function of module scipy.optimize). However, it could be found that this rule could not reproduce observed large variations in m_{rc525}. It was realized that the volume mixing rule would oversimplify the interactions in complex mixture with respect to aerosol refractive index (Liu and Daum, 2008). This was confirmed by a few aerosol refractive index studies (Zhao et al., 2019a).
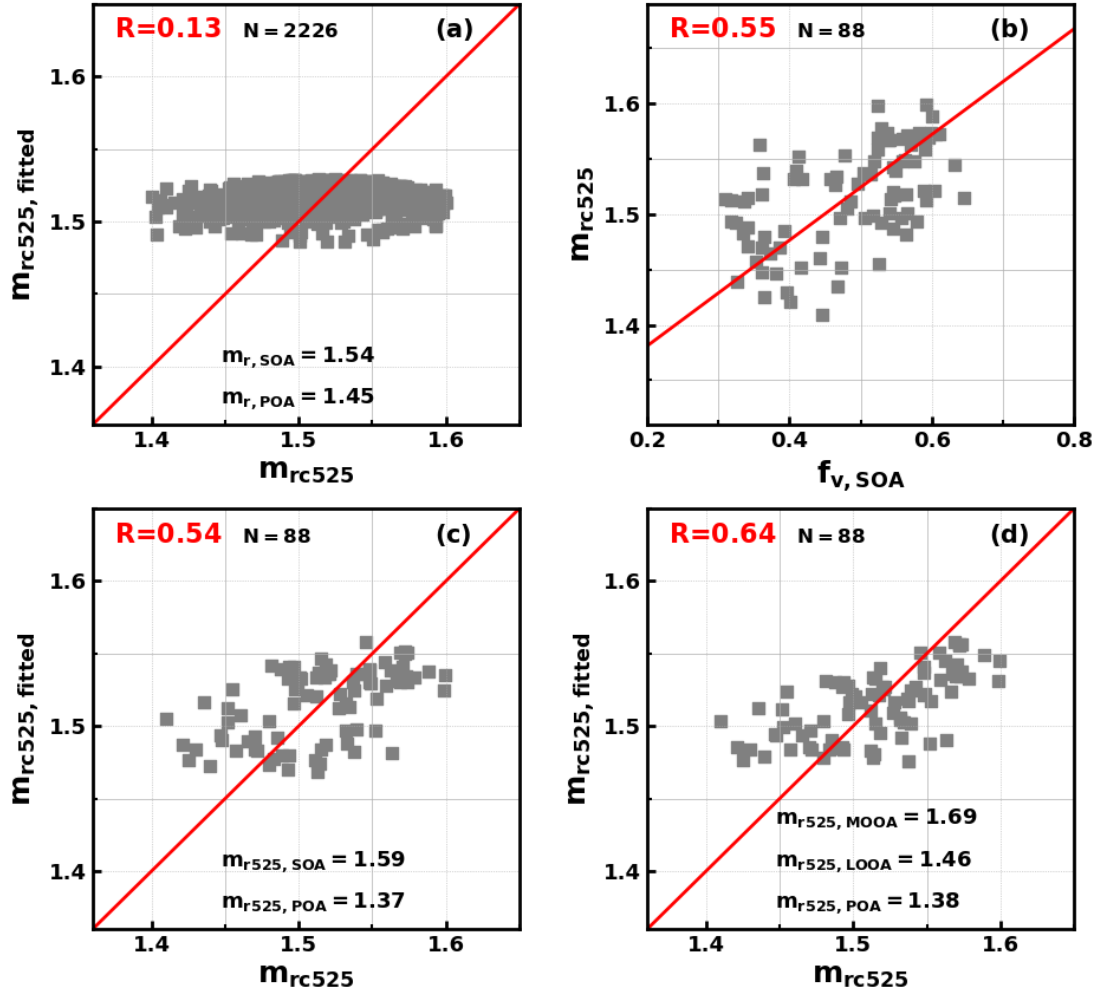
Figure 6. **(a)**Comparison between m_{rc525} and fitted m_{r525} using the volume mixing rule, N is the sample number; **(b)** Relationships between m_{rc525} and volume fractions of SOA in NR-PM$_1$ (f$_{v,SOA}$) when OA volume fractions in NR-PM$_1$ is higher than 75%; **(c)**Comparisons between m_{rc525} and fitted m_{r525} for points in (b) using the volume mixing rule; **(d)** Comparisons between m_{rc525} and fitted m_{r525} for points in (b) using the volume mixing rule, while LOOA and MOOA are treated separately. Red lines indicate the 1:1 reference lines.

447   If we focus on periods when OA dominates aerosol volume (OA volume in total NR-PM$_1$
448   accounts for more than 75%), m_{rc525} shows clear and almost linear trend with the volume fractions of
449   SOA in NR-PM$_1$ as shown in Fig.4b. The question remains whether the volume mixing rule can be
450   used to retrieve m_{rc525} of POA and SOA from these organic aerosol-dominant points. The analysis
451   in Sect. 3.1 demonstrates that the mass concentration of resolved PNSD factor that related with primary
452   sources could mostly be explained by POA and BC, meaning that PNSD and of primary sources and
453   secondary sources could be generally separated in the PMF procedure, suggesting that POA and SOA
454   are likely prone to externally mixed. This could be explained by that the observation site is located
455   near POA source regions in an urban area. This indicates that POA and SOA tend to be optically

independent at the single-particle level. The optical test experiment introduced in Sect. S6 demonstrate that the volume mixing rule can generally be used to retrieve m_{rc525} of POA and SOA if aerosol particles of SOA and POA are externally mixed. In view of this, the volume mixing rule was further applied to scenarios when OA volume dominates (data points in Fig.4b), meaning that effects of other chemical components are minimized. The overall m_{rc525} changes were captured by the fitting while retrieved values for $m_{rc525,POA}$ and $m_{rc525,SOA}$ are 1.37 ± 0.026 and 1.59 ± 0.017 as shown in Fig.4c. The relatively small uncertainty ranges for estimated $m_{rc525,POA}$ and $m_{rc525,SOA}$ confirms the quantitative difference between $m_{rc525,POA}$ and $m_{rc525,SOA}$. For the average PNSD in the retrievals, increase m_{rc525} from 1.37 to 1.59 would result in an ~60% increase of aerosol scattering, which is significant for aerosol radiative forcing estimations (Kuang et al., 2015). Models that assume $m_{r,POA}$ to 1.63 and $m_{r,SOA}$ to 1.43 which is contrary to the finding here, would inevitably results significant bias in organic aerosol radiative forcing estimations (Curci et al., 2019). Based on the above analysis, $m_{r,SOA}$ and $m_{r,POA}$ of 1.37 and 1.59 might be better choice for model settings in regions share similar emissions and meteorological conditions with the observation site.

Considering that O/C of LOOA and MOOA differ much (0.6 vs 1.27) during the long-term campaign. If SOA was further treated separately as LOOA and MOOA in the fitting, extending the volume mixing rule formula as: $m_{r525} = \varepsilon_{AN} \times m_{rc525,AN} + \varepsilon_{AS} \times m_{rc525,AS} + \varepsilon_{AC} \times m_{rc525,AC} + \varepsilon_{POA} \times m_{rc525,POA} + \varepsilon_{LOOA} \times m_{rc525,LOOA} + \varepsilon_{MOOA} \times m_{rc525,MOOA}$,a better correlation coefficient could be achieved as shown in Fig.4d. Note that LOOA and MOOA are generally not externally mixed and likely be prone to internally mixed on the basis of knowledge about organic aerosol aging chain (Jimenez et al., 2009), therefore the volume mixing rule is likely not applicable, and the retrieved results serves better for qualitatively analysis. Retrieved $m_{rc525,POA}$ of 1.38 ± 0.024, and retrieved $m_{rc525,LOOA}$ and $m_{rc525,MOOA}$ of 1.46 ± 0.069 and 1.69 ± 0.059, consistent with the speculations in Sect 3.2 that $m_{r,MOOA}$ is likely substantially higher than $m_{r,LOOA}$ (Fig.S11), although significant retrieval bias of $m_{rc525,LOOA}$ and $m_{rc525,MOOA}$. The retrieved $m_{rc525,LOOA}$ and $m_{rc525,MOOA}$ of 1.46 and 1.69 have a remarkable difference with those ($m_{r,LOOA}$ and $m_{r,MOOA}$ of 1.56 and 1.57) predicted with their O/C and H/C ratios as inputs of the scheme proposed by Li, et al. (2023b). This result suggests that qualitatively, m_r increase with oxidation degree of SOA. Previous laboratory results demonstrate that m_r could increase (Li et al., 2019;He et al., 2022) or decrease (He et al., 2018) with O/C depending on aerosol types, precursors and oxidation conditions. However, as summarized in Moise et al. (2015) , most existing laboratory studies that conducted in the context of gas-phase reactions reveal thatthe increase of O/C would generally decrease m_r at the O/C range of LOOA and

488 MOOA of this study (0.6 to 1.27~~, and m_r from 1.46 to 1.69). This~~). The finding here is likely

489 associated with that MOOA in Guangzhou urban area is mainly formed through multiphase reactions

490 (Zhai et al., 2023) thus ~~has~~it is expected to have higher m_r, as demonstrated by Li et al. (2017)~~that~~

491 ~~multiphase reactions enhance m_r. Most laboratory studies on evolution of $m_{r,SOA}$ were conducted in~~

492 ~~the context of gas-phase reactions, However, for humid regions such as southern China, multiphase~~

493 ~~reactions likely prevail (Zhou et al., 2020;Xu et al., 2020).~~.

4 Conclusions

496   This study thoroughly leverages field measurements and multiple analytical techniques to

497 constrain the real part of the scattering refractive index of organic aerosols. The results reveal

498 substantially higher values for SOA compared to POA, helping to clarify a longstanding discrepancy

499 in their optical properties. The m_r is a fundamental parameter for accurate simulations of aerosol

500 optical properties and their roles in visibility degradation and direct aerosol radiative forcing. In

501 addition, aerosol optical properties are also key for radiative flux simulations which are fundamental

502 for atmospheric photochemistry (Tao et al., 2014;Tian et al., 2019). Therefore, results of studies have

503 both significant implications in environmental and climate issues.

504   Results of Redemann et al. (2000) demonstrate that 5% variation in m_r can lead to approximately

505 30% change in the radiative flux change at the top of atmosphere. Li et al. (2021) further demonstrated

506 for $m_{r,OA}$ changing from 1.3 to 1.65, stratospheric aerosol optical depth relatively changed from −20%

507 to +50%, and caused up to ±100% variability in shortwave radiative forcing, which matters more than

508 mixing state. While OA are mainly composed of POA and SOA, and they both are major components

509 of atmospheric aerosols, therefore accurate representations of $m_{r,POA}$ and $m_{r,SOA}$ are essential for

510 accurate simulations of direct aerosol radiative effects whose uncertainties are the second largest

511 contributions to overall climate forcing estimations (IPCC,AR6, 2023). Our long-term field

512 observation results suggest that utilizing constant values for $m_{r,OA}$ in models would lead to either

513 significant underestimations or overestimations in scattering coefficient therefore significant

514 deviations in estimations of direct aerosol radiative effects. The used constant value is another issue,

515 as presented by Tsigaridis and Kanakidou (2018), most models use 1.53 as $m_{r,OA}$ which is generally

516 appropriate on the basis of this study if $m_{r,OA}$ has to be assumed. While some models even use a

517 constant, for example 1.45 for both SOA and POA which might cause systematical underestimation

518 of OA scattering (Aouizerats et al., 2010;Ma et al., 2012b). If OA is further categorized into SOA and

519 POA in models as applied in Curci, et al. (2019), the appropriate $m_{r,POA}$ and $m_{r,SOA}$ should be used.

520   Large bias would be expected if $m_{r,POA}$ and $m_{r,SOA}$ are set to 1.63 and 1.43 as those in Curci, et al.

521   (2019). In addition, in most models, element ratios of organic components are not available, and

522   organic aerosols are generally categorized as several types of POA and SOA, and SOA are generally

523   treated as a whole in these models (Zhang et al., 2023;Pöhlker et al., 2023). Therefore, $m_{r,POA}$ and

524     $m_{r,SOA}$ values of 1.37 and 1.59 retrieved at 525 nm in this study are recommended for regions share

525   similar emissions and meteorological conditions with the observation site.

526   It should be noteworthy that the POA in this study are primarily composed of fossil combustion

527   from traffic and cooking related organic aerosols, however, organic aerosols directly emitted from

528   biomass burning (BBOA) and other fossil combustions sources such as coal burning also represent a

529   major POA source. Mathai et al. (2023) reported m_r of homogeneously and inhomogeneously mixed

530   tar balls in the free troposphere from biomass burnings as 1.26 and 1.4, which is close to the

531   recommended $m_{r,POA}$. However, results of Womack et al. (2021) reported that m_r of biomass burning

532   aerosols at 475 nm could be higher than 1.6. Results of Luo et al. (2022) further demonstrated that m_r

533   of BBOA might vary a lot and depends highly on combustion conditions. Accurate representations of

534     $m_{r,BBOA}$ stand as urgent need, considering the increasing trends of biomass burning events under

535   background of current global warming. However, the biggest challenge lies in accurate representations

536   of organic aerosols m_r due to $m_{r,SOA}$ variations, because SOA could be formed through varying

537   pathways (condensational growth or multiphase reactions) of different precursor sources volatile

538   organic compounds (biogenic versus anthropogenic), and existing results already proved that SOA

539   formed from varying precursors and pathways has distinct m_r. Therefore, recommend value of $m_{r,SOA}$

540   in this study might represent more the m_r of SOA that formed from anthropogenic precursors in urban

541   and humid regions. Overall, results of this study, underscore the substantially higher $m_{r,SOA}$ than

542     $m_{r,POA}$, not the case currently assumed in models.

543   In addition, results of this study imply that m_r likely increased oxidation level, suggesting crucial

544   impacts of SOA formation mechanisms on m_r variations. Future studies should further examine

545   variations and evolution of $m_{r,SOA}$ than $m_{r,POA}$ under different emissions characteristics and

546   chemistry pathways for reducing uncertainties of direct aerosol radiative effects simulations in

547   chemical, weather and climate models.

548

549

550

551

552

553

554

Competing interests. The contact author has declared that none of the authors has any competing interests.

557

Data Availability. All data presented in Figures of this manuscript are freely available at https://doi.org/10.5281/zenodo.15786937, and more specific raw data will be made available on request due to the data restriction policy.

561

Author Contributions. YK and LL designed the two field campaigns; YK conceived and led this research. LL, BL, JLS, HX, GZ, FLY, MMZ, FL and YK performed measurements of aerosol physical and chemical properties. TD and XD supported this campaign. JLS performed the analysis with YK and LL, JLS and YK wrote the manuscript. All authors contributed to revisions of this paper.

566

Financial support. This work is supported by National Natural Science Foundation of China (42175083, 42105092), the Guangdong Basic and Applied Basic Research Foundation (2025A1515011641) and Fundamental Research Funds for the Central Universities.

570

References:

Aldhaif, A. M., Stahl, C., Braun, R. A., Moghaddam, M. A., Shingler, T., Crosbie, E., Sawamura, P., Dadashazar, H., Ziemba, L., Jimenez, J. L., Campuzano-Jost, P., and Sorooshian, A.: Characterization of the Real Part of Dry Aerosol Refractive Index Over North America From the Surface to 12 km, Journal of Geophysical Research: Atmospheres, 123, 8283-8300, https://doi.org/10.1029/2018JD028504, 2018.

Aouizerats, B., Thouron, O., Tulet, P., Mallet, M., Gomes, L., and Henzing, J. S.: Development of an online radiative module for the computation of aerosol optical properties in 3-D atmospheric models: validation during the EUCAARI campaign, Geosci. Model Dev., 3, 553-564, 10.5194/gmd-3-553-2010, 2010.

Benko, D., Molnár, A., and Imre, K.: Study on the size dependence of complex refractive index of atmospheric aerosol particles over Central Europe, IDOJARAS, 113, 157-175, 2009.

Bohren, C. F., and Huffman, D. R.: Absorption and Scattering by a Sphere, in: Absorption and Scattering of Light by Small Particles, 82-129, 1998.

Cai, J., Chu, B., Yao, L., Yan, C., Heikkinen, L. M., Zheng, F., Li, C., Fan, X., Zhang, S., Yang, D., Wang, Y., Kokkonen, T. V., Chan, T., Zhou, Y., Dada, L., Liu, Y., He, H., Paasonen, P., Kujansuu, J. T., Petäjä, T., Mohr, C., Kangasluoma, J., Bianchi, F., Sun, Y., Croteau, P. L., Worsnop, D. R., Kerminen, V.-M., Du, W., Kulmala, M., and Daellenbach, K. R.: Size-segregated particle number and mass concentrations from different emission sources in urban Beijing, Atmospheric Chemistry and Physics, 20, 12721-12740, 10.5194/acp-20-12721-2020, 2020a.

Cai, J., Chu, B., Yao, L., Yan, C., Heikkinen, L. M., Zheng, F., Li, C., Fan, X., Zhang, S., Yang, D., Wang, Y., Kokkonen, T. V., Chan, T., Zhou, Y., Dada, L., Liu, Y., He, H., Paasonen, P., Kujansuu, J. T., Petäjä, T., Mohr, C., Kangasluoma, J., Bianchi, F., Sun, Y., Croteau, P. L., Worsnop, D. R., Kerminen, V. M., Du, W., Kulmala, M., and Daellenbach, K. R.: Size-segregated particle number and mass concentrations from different emission sources in urban Beijing, Atmos. Chem. Phys., 20, 12721-12740, 10.5194/acp-20-12721-2020, 2020b.

Canonaco, F., Crippa, M., Slowik, J. G., Baltensperger, U., and Prévôt, A. S. H.: SoFi, an IGOR-based interface for the efficient use of the generalized multilinear engine (ME-2) for the source apportionment: ME-2 application to aerosol mass spectrometer data, Atmos. Meas. Tech., 6, 3649-3661, 10.5194/amt-6-3649-2013, 2013.

Canonaco, F., Tobler, A., Chen, G., Sosedova, Y., Slowik, J. G., Bozzetti, C., Daellenbach, K. R., El Haddad, I., Crippa, M., Huang, R. J., Furger, M., Baltensperger, U., and Prévôt, A. S. H.: A new method for long-term source apportionment with time-dependent factor profiles and uncertainty assessment using SoFi Pro: application to 1 year of organic aerosol data, Atmos. Meas. Tech., 14, 923-943, 10.5194/amt-14-923-2021, 2021.

Cheng, Y. F., Berghof, M., Garland, R. M., Wiedensohler, A., Wehner, B., Müller, T., Su, H., Zhang, Y. H., Achtert, P., Nowak, A., Pöschl, U., Zhu, T., Hu, M., and Zeng, L. M.: Influence of soot mixing state on aerosol light absorption and single scattering albedo during air mass aging at a polluted regional site in northeastern China, Journal of Geophysical Research: Atmospheres, 114, https://doi.org/10.1029/2008JD010883, 2009.

Curci, G., Alyuz, U., Barò, R., Bianconi, R., Bieser, J., Christensen, J. H., Colette, A., Farrow, A., Francis, X., Jiménez-Guerrero, P., Im, U., Liu, P., Manders, A., Palacios-Peña, L., Prank, M., Pozzoli, L., Sokhi, R., Solazzo, E., Tuccella, P., Unal, A., Vivanco, M. G., Hogrefe, C., and Galmarini, S.: Modelling black carbon absorption of solar radiation: combining external and internal mixing assumptions, Atmos. Chem. Phys., 19, 181-204, 10.5194/acp-19-181-2019, 2019.

Drinovec, L., Močnik, G., Zotter, P., Prévôt, A. S. H., Ruckstuhl, C., Coz, E., Rupakheti, M., Sciare, J., Müller, T., Wiedensohler, A., and Hansen, A. D. A.: The "dual-spot" Aethalometer: an improved measurement of aerosol black carbon with real-time loading compensation, Atmospheric Measurement Techniques, 8, 1965-1979, 10.5194/amt-8-1965-2015, 2015.

Guo, J., Zhou, S., Cai, M., Zhao, J., Song, W., Zhao, W., Hu, W., Sun, Y., He, Y., Yang, C., Xu, X., Zhang, Z., Cheng, P., Fan, Q., Hang, J., Fan, S., Wang, X., and Wang, X.: Characterization of submicron particles by time-of-flight aerosol chemical speciation monitor (ToF-ACSM) during wintertime: aerosol composition, sources, and chemical processes in Guangzhou, China, Atmospheric Chemistry and Physics, 20, 7595-7615, 10.5194/acp-20-7595-2020, 2020.

He, Q., Bluvshtein, N., Segev, L., Meidan, D., Flores, J. M., Brown, S. S., Brune, W., and Rudich, Y.: Evolution of the Complex Refractive Index of Secondary Organic Aerosols during Atmospheric Aging, Environmental science & technology, 52, 3456-3465, 10.1021/acs.est.7b05742, 2018.

He, Q., Li, C., Siemens, K., Morales, A. C., Hettiyadura, A. P. S., Laskin, A., and Rudich, Y.: Optical Properties of Secondary Organic Aerosol Produced by Photooxidation of Naphthalene under NOx Condition, Environmental science & technology, 56, 4816-4827, 10.1021/acs.est.1c07328, 2022.

Hoffer, A., Tóth, Á., Pósfai, M., Chung, C. E., and Gelencsér, A.: Brown carbon absorption in the red and near-infrared spectral region, Atmos. Meas. Tech., 10, 2353-2359, 10.5194/amt-10-2353-2017, 2017.

IPCC,AR6: The Earth's Energy Budget, Climate Feedbacks and Climate Sensitivity, in: Climate Change 2021 – The Physical Science Basis: Working Group I Contribution to the Sixth Assessment Report of the Intergovernmental Panel on Climate Change, edited by: Intergovernmental Panel on Climate, C., Cambridge University Press, Cambridge, 923-1054, 2023.

Jarzembski, M. A., Norman, M. L., Fuller, K. A., Srivastava, V., and Cutten, D. R.: Complex refractive index of ammonium nitrate in the 2–20-µm spectral range, Appl. Opt., 42, 922-930, 10.1364/AO.42.000922, 2003.

Jimenez, J. L., Canagaratna, M. R., Donahue, N. M., Prevot, A. S. H., Zhang, Q., Kroll, J. H., DeCarlo, P. F., Allan, J. D., Coe, H., Ng, N. L., Aiken, A. C., Docherty, K. S., Ulbrich, I. M., Grieshop, A. P., Robinson, A. L., Duplissy, J., Smith, J. D., Wilson, K. R., Lanz, V. A., Hueglin, C., Sun, Y. L., Tian, J., Laaksonen, A., Raatikainen, T., Rautiainen, J., Vaattovaara, P., Ehn, M., Kulmala, M., Tomlinson, J. M., Collins, D. R., Cubison, M. J., Dunlea, J., Huffman, J. A., Onasch, T. B., Alfarra, M. R., Williams, P. I., Bower, K., Kondo, Y., Schneider, J., Drewnick, F., Borrmann, S., Weimer, S., Demerjian, K., Salcedo, D., Cottrell, L., Griffin, R., Takami, A., Miyoshi, T., Hatakeyama, S., Shimono, A., Sun, J. Y., Zhang, Y. M., Dzepina, K., Kimmel, J. R., Sueper, D., Jayne, J. T., Herndon, S. C., Trimborn, A. M., Williams, L. R., Wood, E. C., Middlebrook, A. M., Kolb, C. E., Baltensperger, U., and Worsnop, D. R.: Evolution of Organic Aerosols in the Atmosphere, Science, 326, 1525-1529, 10.1126/science.1180353, 2009.

Kanakidou, M., Seinfeld, J. H., Pandis, S. N., Barnes, I., Dentener, F. J., Facchini, M. C., Van Dingenen, R., Ervens, B., Nenes, A., Nielsen, C. J., Swietlicki, E., Putaud, J. P., Balkanski, Y., Fuzzi, S., Horth, J., Moortgat, G. K., Winterhalter, R., Myhre, C. E. L., Tsigaridis, K., Vignati, E., Stephanou, E. G., and Wilson, J.: Organic aerosol and global climate modelling: a review, Atmos. Chem. Phys., 5, 1053-1123, 10.5194/acp-5-1053-2005, 2005.

Kim, H., Liu, S., Russell, L. M., and Paulson, S. E.: Dependence of Real Refractive Indices on O:C, H:C and Mass Fragments of Secondary Organic Aerosol Generated from Ozonolysis and Photooxidation of Limonene and α-Pinene, Aerosol Science and Technology, 48, 498-507, 10.1080/02786826.2014.893278, 2014.

Kuang, Y., Zhao, C. S., Tao, J. C., and Ma, N.: Diurnal variations of aerosol optical properties in the North China Plain and their influences on the estimates of direct aerosol radiative effect, Atmos. Chem. Phys., 15, 5761-5772, 10.5194/acp-15-5761-2015, 2015.

Kuang, Y., Zhao, C. S., Zhao, G., Tao, J. C., Xu, W., Ma, N., and Bian, Y. X.: A novel method for calculating ambient aerosol liquid water content based on measurements of a humidified nephelometer system, Atmospheric Measurement Techniques, 11, 2967-2982, 10.5194/amt-11-2967-2018, 2018.

Kuang, Y., Huang, S., Xue, B., Luo, B., Song, Q., Chen, W., Hu, W., Li, W., Zhao, P., Cai, M., Peng, Y., Qi, J., Li, T., Wang, S., Chen, D., Yue, D., Yuan, B., and Shao, M.: Contrasting effects of secondary

organic aerosol formations on organic aerosol hygroscopicity, Atmos. Chem. Phys., 21, 10375-10391, 10.5194/acp-21-10375-2021, 2021.

Kuang, Y., Xu, W., Tao, J., Luo, B., Liu, L., Xu, H., Xu, W., Xue, B., Zhai, M., Liu, P., and Sun, Y.: Divergent Impacts of Biomass Burning and Fossil Fuel Combustion Aerosols on Fog-Cloud Microphysics and Chemistry: Novel Insights From Advanced Aerosol-Fog Sampling, Geophysical Research Letters, 51, e2023GL107147, https://doi.org/10.1029/2023GL107147, 2024.

Lambe, A. T., Cappa, C. D., Massoli, P., Onasch, T. B., Forestieri, S. D., Martin, A. T., Cummings, M. J., Croasdale, D. R., Brune, W. H., Worsnop, D. R., and Davidovits, P.: Relationship between Oxidation Level and Optical Properties of Secondary Organic Aerosol, Environmental science & technology, 47, 6349-6357, 10.1021/es401043j, 2013.

Li, C., He, Q., Schade, J., Passig, J., Zimmermann, R., Meidan, D., Laskin, A., and Rudich, Y.: Dynamic changes in optical and chemical properties of tar ball aerosols by atmospheric photochemical aging, Atmos. Chem. Phys., 19, 139-163, 10.5194/acp-19-139-2019, 2019.

Li, F., Luo, B., Zhai, M., Liu, L., Zhao, G., Xu, H., Deng, T., Deng, X., Tan, H., Kuang, Y., and Zhao, J.: Black carbon content of traffic emissions significantly impacts black carbon mass size distributions and mixing states, Atmos. Chem. Phys., 23, 6545-6558, 10.5194/acp-23-6545-2023, 2023a.

Li, K., Li, J., Liggio, J., Wang, W., Ge, M., Liu, Q., Guo, Y., Tong, S., Li, J., Peng, C., Jing, B., Wang, D., and Fu, P.: Enhanced Light Scattering of Secondary Organic Aerosols by Multiphase Reactions, Environmental science & technology, 51, 1285-1292, 10.1021/acs.est.6b03229, 2017.

Li, Y., Dykema, J., Deshler, T., and Keutsch, F.: Composition Dependence of Stratospheric Aerosol Shortwave Radiative Forcing in Northern Midlatitudes, Geophysical Research Letters, 48, e2021GL094427, https://doi.org/10.1029/2021GL094427, 2021.

Li, Y., Bai, B., Dykema, J., Shin, N., Lambe, A. T., Chen, Q., Kuwata, M., Ng, N. L., Keutsch, F. N., and Liu, P.: Predicting Real Refractive Index of Organic Aerosols From Elemental Composition, Geophysical Research Letters, 50, 10.1029/2023gl103446, 2023b.

Li, Y., Bai, B., Dykema, J., Shin, N., Lambe, A. T., Chen, Q., Kuwata, M., Ng, N. L., Keutsch, F. N., and Liu, P.: Predicting Real Refractive Index of Organic Aerosols From Elemental Composition, Geophysical Research Letters, 50, e2023GL103446, https://doi.org/10.1029/2023GL103446, 2023c.

Lide, D. R.: CRC handbook of chemistry and physics, CRC press, 2004.

Liu, L., Kuang, Y., Zhai, M., Xue, B., He, Y., Tao, J., Luo, B., Xu, W., Tao, J., Yin, C., Li, F., Xu, H., Deng, T., Deng, X., Tan, H., and Shao, M.: Strong light scattering of highly oxygenated organic aerosols impacts significantly on visibility degradation, Atmos. Chem. Phys., 22, 7713-7726, 10.5194/acp-22-7713-2022, 2022.

Liu, P., Zhang, Y., and Martin, S. T.: Complex Refractive Indices of Thin Films of Secondary Organic Materials by Spectroscopic Ellipsometry from 220 to 1200 nm, Environmental science & technology, 47, 13594-13601, 10.1021/es403411e, 2013.

Liu, Y., and Daum, P. H.: Relationship of refractive index to mass density and self-consistency of mixing rules for multicomponent mixtures like ambient aerosols, Journal of Aerosol Science, 39, 974-986, https://doi.org/10.1016/j.jaerosci.2008.06.006, 2008.

Luo, B., Kuang, Y., Huang, S., Song, Q., Hu, W., Li, W., Peng, Y., Chen, D., Yue, D., Yuan, B., and Shao, M.: Parameterizations of size distribution and refractive index of biomass burning organic aerosol with black carbon content, Atmos. Chem. Phys., 22, 12401-12415, 10.5194/acp-22-12401-2022, 2022.

Müller, T., Laborde, M., Kassell, G., and Wiedensohler, A.: Design and performance of a three-wavelength LED-based total scatter and backscatter integrating nephelometer, Atmos. Meas. Tech., 4, 1291-1303, 10.5194/amt-4-1291-2011, 2011.

Ma, N., Zhao, C. S., Nowak, A., Müller, T., Pfeifer, S., Cheng, Y. F., Deng, Z. Z., Liu, P. F., Xu, W. Y., Ran, L., Yan, P., Göbel, T., Hallbauer, E., Mildenberger, K., Henning, S., Yu, J., Chen, L. L., Zhou, X. J., Stratmann, F., and Wiedensohler, A.: Aerosol optical properties in the North China Plain during

HaChi campaign: an in-situ optical closure study, Atmos. Chem. Phys., 11, 5959-5973, 10.5194/acp-11-5959-2011, 2011.

Ma, N., Zhao, C. S., Müller, T., Cheng, Y. F., Liu, P. F., Deng, Z. Z., Xu, W. Y., Ran, L., Nekat, B., van Pinxteren, D., Gnauk, T., Müller, K., Herrmann, H., Yan, P., Zhou, X. J., and Wiedensohler, A.: A new method to determine the mixing state of light absorbing carbonaceous using the measured aerosol optical properties and number size distributions, Atmos. Chem. Phys., 12, 2381-2397, 10.5194/acp-12-2381-2012, 2012a.

Ma, X., Yu, F., and Luo, G.: Aerosol direct radiative forcing based on GEOS-Chem-APM and uncertainties, Atmos. Chem. Phys., 12, 5563-5581, 10.5194/acp-12-5563-2012, 2012b.

Mathai, S., Veghte, D., Kovarik, L., Mazzoleni, C., Tseng, K.-P., Bucci, S., Capek, T., Cheng, Z., Marinoni, A., and China, S.: Optical Properties of Individual Tar Balls in the Free Troposphere, Environmental science & technology, 57, 16834-16842, 10.1021/acs.est.3c03498, 2023.

McMeeking, G. R., Kreidenweis, S. M., Carrico, C. M., Collett, J. L., Day, D. E., and Malm, W. C.: Observations of smoke-influenced aerosol during the Yosemite Aerosol Characterization Study: 2. Aerosol scattering and absorbing properties, Journal of Geophysical Research: Atmospheres, 110, 10.1029/2004jd005624, 2005.

Moise, T., Flores, J. M., and Rudich, Y.: Optical Properties of Secondary Organic Aerosols and Their Changes by Chemical Processes, Chemical Reviews, 115, 4400-4439, 10.1021/cr5005259, 2015.

Ouimette, J. R., and Flagan, R. C.: The extinction coefficient of multicomponent aerosols, Atmospheric Environment (1967), 16, 2405-2419, https://doi.org/10.1016/0004-6981(82)90131-7, 1982.

Pöhlker, M. L., Pöhlker, C., Quaas, J., Mülmenstädt, J., Pozzer, A., Andreae, M. O., Artaxo, P., Block, K., Coe, H., Ervens, B., Gallimore, P., Gaston, C. J., Gunthe, S. S., Henning, S., Herrmann, H., Krüger, O. O., McFiggans, G., Poulain, L., Raj, S. S., Reyes-Villegas, E., Royer, H. M., Walter, D., Wang, Y., and Pöschl, U.: Global organic and inorganic aerosol hygroscopicity and its effect on radiative forcing, Nature communications, 14, 6139, 10.1038/s41467-023-41695-8, 2023.

Qiao, H., Kuang, Y., Yuan, F., Liu, L., Zhai, M., Xu, H., Zou, Y., Deng, T., and Deng, X.: Unlocking the Mystery of Aerosol Phase Transitions Governed by Relative Humidity History Through an Advanced Outdoor Nephelometer System, Geophysical Research Letters, 51, e2023GL107179, https://doi.org/10.1029/2023GL107179, 2024.

Redemann, J., Turco, R. P., Liou, K. N., Hobbs, P. V., Hartley, W. S., Bergstrom, R. W., Browell, E. V., and Russell, P. B.: Case studies of the vertical structure of the direct shortwave aerosol radiative forcing during TARFOX, Journal of Geophysical Research: Atmospheres, 105, 9971-9979, https://doi.org/10.1029/1999JD901042, 2000.

Saleh, R.: From Measurements to Models: Toward Accurate Representation of Brown Carbon in Climate Calculations, Current Pollution Reports, 6, 90-104, 10.1007/s40726-020-00139-3, 2020.

Schuster, G. L., Dubovik, O., Holben, B. N., and Clothiaux, E. E.: Inferring black carbon content and specific absorption from Aerosol Robotic Network (AERONET) aerosol retrievals, Journal of Geophysical Research: Atmospheres, 110, https://doi.org/10.1029/2004JD004548, 2005.

Schwarz, J. P., Gao, R. S., Fahey, D. W., Thomson, D. S., Watts, L. A., Wilson, J. C., Reeves, J. M., Darbeheshti, M., Baumgardner, D. G., Kok, G. L., Chung, S. H., Schulz, M., Hendricks, J., Lauer, A., Kärcher, B., Slowik, J. G., Rosenlof, K. H., Thompson, T. L., Langford, A. O., Loewenstein, M., and Aikin, K. C.: Single-particle measurements of midlatitude black carbon and light-scattering aerosols from the boundary layer to the lower stratosphere, Journal of Geophysical Research: Atmospheres, 111, D16207, 10.1029/2006JD007076, 2006.

Stelson, A. W.: Urban aerosol refractive index prediction by partial molar refraction approach, Environmental science & technology, 24, 1676-1679, 1990.

Sun, Y. L., Zhang, Q., Schwab, J. J., Yang, T., Ng, N. L., and Demerjian, K. L.: Factor analysis of combined organic and inorganic aerosol mass spectra from high resolution aerosol mass spectrometer measurements, Atmos. Chem. Phys., 12, 8537-8551, 10.5194/acp-12-8537-2012, 2012.

Tang, I. N.: Chemical and size effects of hygroscopic aerosols on light scattering coefficients, Journal of Geophysical Research: Atmospheres, 101, 19245-19250, https://doi.org/10.1029/96JD03003, 1996.

Tao, J. C., Zhao, C. S., Ma, N., and Liu, P. F.: The impact of aerosol hygroscopic growth on the single-scattering albedo and its application on the NO2 photolysis rate coefficient, Atmos. Chem. Phys., 14, 12055-12067, 10.5194/acp-14-12055-2014, 2014.

Tian, R., Ma, X., Jia, H., Yu, F., Sha, T., and Zan, Y.: Aerosol radiative effects on tropospheric photochemistry with GEOS-Chem simulations, Atmospheric Environment, 208, 82-94, https://doi.org/10.1016/j.atmosenv.2019.03.032, 2019.

Tsigaridis, K., and Kanakidou, M.: The Present and Future of Secondary Organic Aerosol Direct Forcing on Climate, Current Climate Change Reports, 4, 84-98, 10.1007/s40641-018-0092-3, 2018.

Wexler, A. S., and Clegg, S. L.: Atmospheric aerosol models for systems including the ions H+, NH4+, Na+, SO42−, NO3−, Cl−, Br−, and H2O, Journal of Geophysical Research: Atmospheres, 107, ACH 14-11-ACH 14-14, 10.1029/2001jd000451, 2002.

Womack, C. C., Manfred, K. M., Wagner, N. L., Adler, G., Franchin, A., Lamb, K. D., Middlebrook, A. M., Schwarz, J. P., Brock, C. A., Brown, S. S., and Washenfelder, R. A.: Complex refractive indices in the ultraviolet and visible spectral region for highly absorbing non-spherical biomass burning aerosol, Atmos. Chem. Phys., 21, 7235-7252, 10.5194/acp-21-7235-2021, 2021.

Wu, Y., Li, J., Xia, Y., Deng, Z., Tao, J., Tian, P., Gao, Z., Xia, X., and Zhang, R.: Size-resolved refractive index of scattering aerosols in urban Beijing: A seasonal comparison, Aerosol Science and Technology, 55, 1070-1083, 10.1080/02786826.2021.1924357, 2021.

Xu, W., Kuang, Y., Bian, Y., Liu, L., Li, F., Wang, Y., Xue, B., Luo, B., Huang, S., Yuan, B., Zhao, P., and Shao, M.: Current Challenges in Visibility Improvement in Southern China, Environmental Science & Technology Letters, 7, 395-401, 10.1021/acs.estlett.0c00274, 2020.

Xu, W., Chen, C., Qiu, Y., Xie, C., Chen, Y., Ma, N., Xu, W., Fu, P., Wang, Z., Pan, X., Zhu, J., Ng, N. L., and Sun, Y.: Size-resolved characterization of organic aerosol in the North China Plain: new insights from high resolution spectral analysis, Environmental Science: Atmospheres, 1, 346-358, 10.1039/d1ea00025j, 2021.

Yuan, J. F., Huang, X. F., Cao, L. M., Cui, J., Zhu, Q., Huang, C. N., Lan, Z. J., and He, L. Y.: Light absorption of brown carbon aerosol in the PRD region of China, Atmos. Chem. Phys., 16, 1433-1443, 10.5194/acp-16-1433-2016, 2016.

Zhai, M., Kuang, Y., Liu, L., He, Y., Luo, B., Xu, W., Tao, J., Zou, Y., Li, F., Yin, C., Li, C., Xu, H., and Deng, X.: Insights into characteristics and formation mechanisms of secondary organic aerosols in the Guangzhou urban area, Atmos. Chem. Phys., 23, 5119-5133, 10.5194/acp-23-5119-2023, 2023.

Zhang, G., Bi, X., Qiu, N., Han, B., Lin, Q., Peng, L., Chen, D., Wang, X., Peng, P., amp, apos, an, Sheng, G., and Zhou, Z.: The real part of the refractive indices and effective densities for chemically segregated ambient aerosols in Guangzhou measured by a single-particle aerosol mass spectrometer, Atmospheric Chemistry and Physics, 16, 2631-2640, 10.5194/acp-16-2631-2016, 2016a.

Zhang, H., Shen, Z., Wei, X., Zhang, M., and Li, Z.: Comparison of optical properties of nitrate and sulfate aerosol and the direct radiative forcing due to nitrate in China, Atmospheric Research, 113, 113-125, https://doi.org/10.1016/j.atmosres.2012.04.020, 2012.

Zhang, Q., Jimenez, J. L., Canagaratna, M. R., Allan, J. D., Coe, H., Ulbrich, I., Alfarra, M. R., Takami, A., Middlebrook, A. M., Sun, Y. L., Dzepina, K., Dunlea, E., Docherty, K., DeCarlo, P. F., Salcedo, D., Onasch, T., Jayne, J. T., Miyoshi, T., Shimono, A., Hatakeyama, S., Takegawa, N., Kondo, Y., Schneider, J., Drewnick, F., Borrmann, S., Weimer, S., Demerjian, K., Williams, P., Bower, K., Bahreini, R., Cottrell, L., Griffin, R. J., Rautiainen, J., Sun, J. Y., Zhang, Y. M., and Worsnop, D. R.: Ubiquity and dominance of oxygenated species in organic aerosols in anthropogenically-influenced Northern Hemisphere midlatitudes, Geophysical Research Letters, 34, n/a-n/a, 10.1029/2007GL029979, 2007.

Zhang, S., Shen, X., Sun, J., Zhang, Y., Zhang, X., Xia, C., Hu, X., Zhong, J., Wang, J., and Liu, S.: Atmospheric Particle Hygroscopicity and the Influence by Oxidation State of Organic Aerosols in

818 Urban   Beijing,   Journal   of   Environmental   Sciences,   124,   544-556,
819 https://doi.org/10.1016/j.jes.2021.11.019, 2023.

820 Zhang, Y., Zhang, Q., Cheng, Y., Su, H., Kecorius, S., Wang, Z., Wu, Z., Hu, M., Zhu, T.,
821 Wiedensohler, A., and He, K.: Measuring the morphology and density of internally mixed black carbon
822 with SP2 and VTDMA: new insight into the absorption enhancement of black carbon in the atmosphere,
823 Atmospheric Measurement Techniques, 9, 1833-1843, 10.5194/amt-9-1833-2016, 2016b.

824 Zhao, G., Tan, T., Zhao, W., Guo, S., Tian, P., and Zhao, C.: A new parameterization scheme for the
825 real part of the ambient urban aerosol refractive index, Atmos. Chem. Phys., 19, 12875-12885,
826 10.5194/acp-19-12875-2019, 2019a.

827 Zhao, G., Tao, J., Kuang, Y., Shen, C., Yu, Y., and Zhao, C.: Role of black carbon mass size
828 distribution in the direct aerosol radiative forcing, Atmos. Chem. Phys., 19, 13175-13188,
829 10.5194/acp-19-13175-2019, 2019b.

830 Zhao, G., Zhao, W., and Zhao, C.: Method to measure the size-resolved real part of aerosol refractive
831 index using differential mobility analyzer in tandem with single-particle soot photometer, Atmos.
832 Meas. Tech., 12, 3541-3550, 10.5194/amt-12-3541-2019, 2019c.

833 Zhao, G., Li, F., and Zhao, C.: Determination of the refractive index of ambient aerosols, Atmospheric
834 Environment, 240, 117800, 10.1016/j.atmosenv.2020.117800, 2020.

835 Zhao, G., Hu, M., Fang, X., Tan, T., Xiao, Y., Du, Z., Zheng, J., Shang, D., Wu, Z., Guo, S., and Zhao,
836 C.: Larger than expected variation range in the real part of the refractive index for ambient aerosols in
837 China,   Science   of   The   Total   Environment,   779,   146443,
838 https://doi.org/10.1016/j.scitotenv.2021.146443, 2021a.

839 Zhao, G., Hu, M., Zhu, W., Tan, T., Shang, D., Zheng, J., Du, Z., Guo, S., Wu, Z., Zeng, L., and Zhao,
840 C.: Parameterization of the ambient aerosol refractive index with source appointed chemical
841 compositions,   Science   of   The   Total   Environment,   842,   156573,
842 https://doi.org/10.1016/j.scitotenv.2022.156573, 2022.

843 Zhao, W., Tan, W., Zhao, G., Shen, C., Yu, Y., and Zhao, C.: Determination of equivalent black carbon
844 mass concentration from aerosol light absorption using variable mass absorption cross section, Atmos.
845 Meas. Tech., 14, 1319-1331, 10.5194/amt-14-1319-2021, 2021b.

846 Zhong, J., Zhang, X., Wang, Y., Wang, J., Shen, X., Zhang, H., Wang, T., Xie, Z., Liu, C., Zhang, H.,
847 Zhao, T., Sun, J., Fan, S., Gao, Z., Li, Y., and Wang, L.: The two-way feedback mechanism between
848 unfavorable meteorological conditions and cumulative aerosol pollution in various haze regions of
849 China, Atmos. Chem. Phys., 19, 3287-3306, 10.5194/acp-19-3287-2019, 2019.

850 Zhou, W., Xu, W., Kim, H., Zhang, Q., Fu, P., Worsnop, D. R., and Sun, Y.: A review of aerosol
851 chemistry in Asia: insights from aerosol mass spectrometer measurements, Environmental Science:
852 Processes & Impacts, 22, 1616-1653, 10.1039/D0EM00212G, 2020.

853 Zhou, Y., Ma, N., Wang, Q., Wang, Z., Chen, C., Tao, J., Hong, J., Peng, L., He, Y., Xie, L., Zhu, S.,
854 Zhang, Y., Li, G., Xu, W., Cheng, P., Kuhn, U., Zhou, G., Fu, P., Zhang, Q., Su, H., and Cheng, Y.:
855 Bimodal distribution of size-resolved particle effective density: results from a short campaign in a rural
856 environment over the North China Plain, Atmos. Chem. Phys., 22, 2029-2047, 10.5194/acp-22-2029-
857 2022, 2022.

858